Coincident observation of air Čerenkov light by a surface array and muon bundles by a deep underground detector

M. Ambrosio,[12] R. Antolini,[7] G. Auriemma,[14,*] R. Baker,[a,11] A. Baldini,[13] B. Bam,[2] G.C. Barbarino,[12] B.C. Barish,[a,4] G. Battistoni,[6,†] R. Bellotti,[1] C. Bemporad,[13] P. Bernardini,[10] H. Bilokon,[6] V. Bisi,[16] C. Bloise,[6] C. Bower,[8] S. Bussino,[14] F. Cafagna,[1] M. Calicchio,[1] D. Campana,[12] M. Carboni,[6] A. Corona,[6] S. Cecchini,[2,‡] F. Cei,[13] V. Chiarella,[6] R. Cormack,[3] S. Coutu,[11] G. DeCataldo,[1] H. Dekhissi,[2,§] C. DeMarzo,[1] M. De Vincenzi,[14,‖] A. Di Credico,[9] E. Diehl,[11] O. Erriquez,[1] C. Favuzzi,[1] C. Forti,[6] P. Fusco,[1] G. Giacomelli,[2] G. Giannini,[13,¶] N. Giglietto,[1] M. Grassi,[13] P. Green,[18] A. Grillo,[6] F. Guarino,[12] P. Guarnaccia,[1] C. Gustavino,[7] A. Habig,[a,8] R. Heinz,[8] J.T. Hong,[4] E. Iarocci,[6,**] E. Katsavounidis,[4] E. Kearns,[3] M. Kertzman,[b,20] S. Kyriazopoulou,[4] E. Lamanna,[14] C. Lane,[5] C. Lee,[11] D.S. Levin,[a,11] P. Lipari,[14] G. Liu,[4] R. Liu,[4] M.J. Longo,[11] Y. Lu,[15] G. Ludlam,[3] G. Mancarella,[10] G. Mandrioli,[2] A. Margiotta-Neri,[2] A. Marin,[3] A. Marini,[6] D. Martello,[10] A. Marzari Chiesa,[16] D.G. Michael,[4] S. Mikheyev,[7,††] L. Miller,[8] M. Mittlebrunn,[5] P. Monacelli,[9] M. Monteno,[16] S. Mufson,[a,8] J. Musser,[a,8] D. Nicoló,[13] R. Nolty,[4] S. Nutter,[11] C. Okada,[3] G. Osteria,[12] O. Palamara,[10] S. Parlati,[7] V. Patera,[6] L. Patrizii,[2] B. Pavesi,[2] R. Pazzi,[13] C.W. Peck,[4] J. Petrakis,[17] S. Petrera,[10] N.D. Pignatano,[4] P. Pistilli,[10] F. Predieri,[2] J. Reynoldson,[7] F. Ronga,[6] G. Sanzani,[2] A. Sanzgiri,[15] C. Satriano,[14*] L. Satta,[6,**] E. Scapparone,[2] K. Scholberg,[4] A. Sciubba,[14,**] G. Sembroski,[b,19] P. Serra Lugaresi,[2] M. Severi,[14] M. Sitta,[16] P. Spinelli,[1] M. Spinetti,[6] M. Spurio,[2] J. Steele,[4] R. Steinberg,[5] J.L. Stone,[3] L.R. Sulak,[3] A. Surdo,[10] G. Tarlé,[a,11] V. Togo,[2] V. Valente,[6] C.W. Walter,[4] R. Webb,[15] and W. Worstell[3]

(GRACE and MACRO Collaborations)

[1] *Dipartimento di Fisica dell'Università di Bari and INFN, Bari, Italy*
[2] *Dipartimento di Fisica dell'Università di Bologna and INFN, Bologna, Italy*
[3] *Physics Department, Boston University, Boston, Massachusetts 02215*
[4] *California Institute of Technology, Pasadena, California 91125*
[5] *Department of Physics, Drexel University, Philadelphia, Pennsylvania 19104*
[6] *Laboratori Nazionali di Frascati dell'INFN, Frascati (Roma), Italy*
[7] *Laboratoire Nazionali del Gran Sasso dell'INFN, Assergi (L'Aquila), Italy*
[8] *Departments of Physics and Astronomy, Indiana University, Bloomington, Indiana 47405*
[9] *Dipartimento di Fisica dell'Università dell'Aquila and INFN, L'Aquila, Italy*
[10] *Dipartimento di Fisica dell'Università di Lecce and INFN, Lecce, Italy*
[11] *Department of Physics, University of Michigan, Ann Arbor, Michigan 48109*
[12] *Dipartimento di Fisica dell'Università di Napoli and INFN, Napoli, Italy*
[13] *Dipartimento di Fisica dell'Università di Pisa and INFN, Pisa, Italy*
[14] *Dipartimento di Fisica dell'Università di Roma and INFN, Roma, Italy*
[15] *Physics Department, Texas A&M University, College Station, Texas 77843*
[16] *Dipartimento di Fisica, dell'Università di Torino and INFN, Torino, Italy*
[17] *Bartol Research Institute, University of Delaware, Newark, Delaware 19716*
[18] *Sandia National Laboratory, Albuquerque, New Mexico 87185*
[19] *Department of Physics, Purdue University, West Lafayette, Indiana 47907*
[20] *Department of Physics, DePauw University, Greencastle, Indiana 46135*

(Received 1 March 1994)

We report on the simultaneous observation of atmospheric Čerenkov light by a prototype five telescope array, GRACE (Gran Sasso Air Čerenkov Experiment) with deep underground muons in the MACRO (Monopole Astrophysics and Cosmic Ray Observatory). The telescope array was deployed at Campo Imperatore above the Gran Sasso Laboratory for a run completed in the fall of 1992. The total live time for the combined surface-underground operation was $\sim$ 100 h during which more than 300 events were seen in coincidence. The efficacy of this technique to monitor the electromagnetic and penetrating muon components of a cosmic-ray-induced cascade is discussed.

PACS number(s): 96.40.De, 29.40.Ka, 96.40.Pq

---

[a] GRACE and MACRO Collaborations.
[b] GRACE Collaboration only.
Absence of a or b: MACRO Collaboration only.
[*] Also at Università della Basilicata, Potenza, Italy.
[†] Also at INFN, Milano, Italy.
[‡] Also at Istitute TESRE/CNR, Bologna, Italy.
[§] Also at Faculty of Sciences, Oujda, Morocco.
[‖] Also at Università di Trieste and INFN, Trieste, Italy.
[¶] Also at Università di Trieste and INFN, Trieste, Italy.
[**] Also at Dipartimento di Energetica, Università di Roma, Roma, Italy.
[††] Also at Institute for Nuclear Research, Russian Academy of Sciences, Moscow.

I. INTRODUCTION

A fundamental problem in ultrahigh energy cosmic ray physics for the past three decades has been the determination of the elemental abundances and spectra of primary particles incident at Earth's atmosphere [1]. This flux of particles represents the end product of a long sequence of processes such as particle production at the source, acceleration and injection into the interstellar medium, propagation through the galactic magnetic field, and spallation due to collisions with matter. Because of the very small fluxes at energies above 10 TeV, direct measurements of cosmic ray composition by balloon or satellite payloads are being extended by indirect methods, generally with large acceptance terrestrial detectors. Such detectors observe not the primary particle, but the hadronic and/or electromagnetic cascade resulting from a collision of the primary projectile with oxygen and nitrogen targets.

Attempts to measure indirectly the cosmic ray composition at energies above 10 TeV are plagued by an incomplete experimental picture of the high energy nucleus-nucleus interaction and resulting cascade. Typically, extensive air shower (EAS) arrays measure electron content and are thus sensitive to the electromagnetic component of the cascade. Air Čerenkov detectors are also sensitive to the electromagnetic component with better sampling statistics but at the cost of reduced live time. Deep underground detectors are often capable of observing deeply penetrating muon bundles [2–8], an interaction product which is sensitive to the type of primary particle [9]. For a specified slant depth of overburden, heavier nuclei produce more muons than protons or light nuclei. The underground muon yield, spatial distribution, and angular distribution also reflect the nature of the interaction. High energy muons normally arise from the decay of charged pions and kaons, which can be considered to be radiated from an excited *isobaric* state of the interacting projectile [10]. At energies near and above the "knee" ($\sim 10^{16}$ eV) of the all-particle spectrum, where knowledge of the inclusive pion production cross sections (and hence muon yield) is limited, various additional muon production mechanisms have been discussed. These mechanisms range from large scaling violations in the Feynman x variable [11] in the forward or high rapidity region to promptly decaying heavy flavor mesons [12]. We finally note that even if the interactions were completely understood, underground muon detectors alone generally lack the means to gauge the primary particle energy.

The role of a coincidence measurement technique is motivated by the above considerations. Simultaneous observation of the surface air shower products with deep underground [at a depth of $\sim$ 4000 meters water equivalent (mwe)] muons allows the muon multiplicity distribution and the muon lateral separation distribution to be assessed as a function of energy. A specific advantage offered by an air Čerenkov detector array is its potential to trigger at low thresholds, perhaps tens of TeV. At energies below $\sim$ 100 TeV the underground muon flux is produced mostly by cosmic ray protons. Nucleons that fragment from heavier nuclei (at the same total energy as a proton) rarely produce muons with sufficient energy ($\sim$ 2 TeV) to survive to a deep detector. Whereas a 60 TeV proton might produce a few such muons, a 60 TeV helium nucleus (15 TeV per nucleon) is much less likely to do so. In Fig. 1 we show how elemental species of increasing atomic number contribute to the production of multiple (two or more) muons at an average MACRO depth of 3700 mwe. These results were obtained from a Monte Carlo–based parametrization of the deep underground muon flux [13] which gives the average number of muons produced by a specified primary at a given zenith angle and slant depth. Folded into this calculation are the approximate relative elemental abundances at 10 TeV. These abundances are based on the extrapolation of somewhat lower energy ($\sim$ 100 GeV) direct measurements [14]. Even with the large uncertainties in this extrapolation it is evident that the single and multiple muon events below 100 TeV are dominated by light nucleus (proton and helium) progenitors. At 100 TeV, for example, the proton contribution to the underground multiple muon flux is about 72%, the helium contribution is about 25%, and the contribution by nuclei heavier than helium is less than 3%. Coincidence Čerenkov light and underground muon observations at this energy regime therefore allow evaluation of aspects of the interaction, i.e., charged particle production and the transverse momentum distribution, largely independent of composition. Cascade simulations that are tuned or otherwise demonstrated to be consistent with the observed underground muon physics in an energy region where the primary composition has little effect might then be more safely extrapolated to higher energies where the composition is not well known.

The motivation for the measurement reported below is

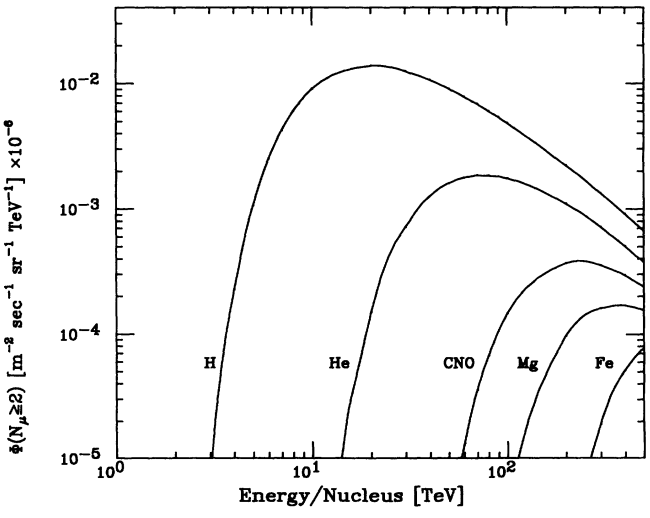

FIG. 1. Expected flux of muon bundles (at least two muons) versus total energy at a depth of 3700 meters water equivalent [mwe] produced by primary species of increasing atomic number. Calculated from reference in text.

to determine the feasibility and utility to simultaneously monitor the Čerenkov and penetrating muon components of a high energy cosmic ray interaction [15,16]. In particular we evaluated the performance of a *unit cell* array of searchlight style [17] Čerenkov light collectors (hereafter referred to simply as telescopes) that could ultimately serve as a prototype for a greatly expanded matrix of telescopes that subtends a large fraction of the acceptance of a deep underground muon detector. An expanded array could provide the required combination of multitelescope sampling of the wave front and an event rate sufficiently high to overcome a small live time fraction. While coincidence measurements of EAS with underground muons have been undertaken [18,19], the Čerenkov technique potentially offers lower thresholds than the ~100–1000 TeV typical of many EAS arrays [20] and therefore affords operation with muon detectors in this otherwise unobservable energy region.

In this paper we report on the initial run of a five element array designed to view EAS Čerenkov light in coincidence with deep underground muons observed with the MACRO detector [21,22] at the Gran Sasso Laboratory.

The goals of this prototype test were the following. To establish unambiguously the feasibility of Čerenkov underground muon coincidence detection with MACRO.

Establish that a reasonable coincidence rate (i.e., a few events per live hour) is obtainable. This implies the ability to trigger at a primary energy much lower than that generally allowed by an EAS array.

Examine the dependence of the Čerenkov light yield (or measured phototube charge) on the distance from the shower core.

Measure arrival direction of the light wave front and check the pointing accuracy of the underground detector.

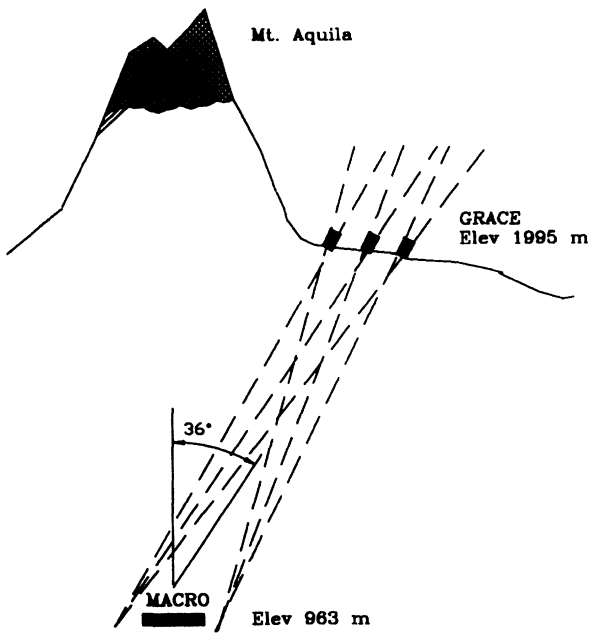

FIG. 2. Profile of GRACE-MACRO configuration.

II. EXPERIMENTAL CONFIGURATION

Complete descriptions of the MACRO detector and GRACE prototype are given elsewhere [21–23]. Our arrangement, shown schematically in Fig. 2, entailed the deployment of medium aperture Čerenkov telescopes on the mountain above the subterranean Gran Sasso Laboratory in central Italy (13.57° E, 42.45° N). A direction vector from the MACRO origin (elevation 963 m above sea level) to the center of GRACE pointed at 36.3° zenith and 206.3° east of north. The elevation of the center of GRACE was 1995 m above sea level at an atmospheric depth 791 $g\,cm^{-2}$ and atmospheric slant depth (in the direction of MACRO, elevation=963 m) of 977 $g\,cm^{-2}$. The distance between GRACE and MACRO was 1280 m, corresponding to 3470 ± 50 mwe. The error reflects the uncertainty in rock density. The alignment of the array's arms (north to south and east to west) was measured by a commercial surveyor contractor with a precision of better than 0.1°. We performed an independent survey of the north-south alignment to less than 0.2°.

A. GRACE

The array staged in the experiment consisted of five light collectors. Four of the telescopes were located on the corners of a square, 80 m on a side, while a fifth was placed at the center. Their optical axes were oriented to the center of MACRO. This configuration serves as basic cell in an expanded array in which several hundred such units distributed over a fraction of a square km would point back to an underground detector. The angular acceptance is uniform for wave fronts arriving off axis up to a half opening angle of 5°, then falls off gradually to zero acceptance at 8°. Each telescope viewed a patch of sky overlapping about 4° with its neighbors.

The optical components of our light collectors consisted of a searchlight style reflector and phototube. The reflector was a 81 cm diameter, 86 cm focal length, parabolic, aluminized glass mirror [24]. Light was focused onto a 20 cm diameter hemispherical EMI phototube.

Phototube signals were routed to amplifiers (gain=20) before discrimination and subsequent trigger formation. The data acquisition was normally triggered when two or more telescopes generated pulses above a fixed electronic threshold within, at most, 400 ns of each other. Because of the varying intensity of ambient light, this threshold was tuned nightly to maintain a manageable acquisition rate on the order of 1–2 Hz. This rate was dictated by the limited data storage capacity. The electronic threshold was typically 50–70 mV after amplification. Each event trigger latched a clock with a 32 μs least count. Our raw timing resolution over the course of a single night's run was ~ 1 ms, but when correction for the thermal drift of the clock was possible, event timing to better than 100 μs was obtained. The intrinsic MACRO trigger formation timing jitter of 1 μs is a negligible component of the overall timing error. Additional information recorded for each trigger was the relative time of arrival

of the Čerenkov pulse at each telescope and the integrated charge observed by each of the phototubes. The time-to-digital converter (TDC) used for time of arrival measurements had a least count of 1 ns.

In order to maintain tolerable photocurrents we operated the phototubes at relatively low gains ($\sim 10^5$–10^6). Even so, photocurrents in excess of 100 μA were produced by the high ambient night sky light. This current tends to limit the dynamic range of the charge measurement, and can degrade phototube performance over a period of months. In the measurements reported here the dynamic range was limited by the full scale of the charge integrating, analogue-to-digital converter (ADC) to under 800 photoelectrons.

B. MACRO

The MACRO detector is located in Hall B of the Gran Sasso underground laboratory. Detailed descriptions of the apparatus are given in Refs. [21] and [22]. Briefly, it is a large area detector equipped with streamer tube chambers, liquid scintillator tanks, and track-etch detectors arranged in a modular structure (supermodules). Each of the six supermodules is 12 m×12 m×9 m in size and consists of a 4.8 m high lower level filled with rock absorber and a 4.2 m high hollow upper level. In this paper, only data from the lower level of the apparatus are included and are described further. Particle tracking is performed with the streamer tubes, which are distributed on ten horizontal planes, separated by $\sim$ 60 cm^{-2} of $CaCO_3$ rock absorbers, and on six planes on each vertical wall. Each streamer tube has a square cross section of 3×3 cm^2, and is 12 m long. For each plane two coordinates are digitally read out, the wire view and the pickup strip view. The pickup aluminum strips are 3 cm wide and are aligned at a stereo angle of 26.5° with respect to the streamer tubes. This arrangement allows a spatial resolution of 1.1 cm in both views, corresponding to an intrinsic angular resolution of 0.2° for muons crossing ten horizontal planes. Tracks on the different views can be associated in space in the majority of events, depending upon the spatial separation and multiplicity. After accounting for multiple Coulomb scattering in the rock overburden the angular resolution [25] for determining the direction of the shower axis is 1.0°, producing a 22 meter uncertainty (one standard deviation) in the location of the shower core at the surface. In the direction of the Čerenkov array, the projected area is $\sim$ 900 m^2, and the trigger efficiency for muons which penetrate MACRO with more than 2 m path length is close to 100%.

III. SIMULATIONS OF THE ČERENKOV SIGNAL

EAS Čerenkov light Monte Carlo calculations [26] have been applied to this telescope configuration in order to determine the expected photoelectron yield. In particular, we are interested in the intensity of Čerenkov light as a function of distance from the core, and in the arrival time profile of the wave front. These simulations, which commence with the injection of a primary proton at the "top" of the atmosphere (at a residual atmosphere of 5 g), generate a three-dimensional electromagnetic cascade and track all charged particles with energy above the critical energy for Čerenkov photon production. The critical energy is both altitude and particle dependent. It is 21 MeV for electrons at sea level. Čerenkov photons radiated in the shower are then propagated through the atmosphere and through the telescope optics. The expected photoelectron radial distributions generated by a 20 TeV proton at vertical and 36° incidence (the approximate angle of the surface array from MACRO) are shown in Fig. 3. These are the parametrized curves for the *mean* photoelectron yield averaged around the core and also over 20 simulated showers. The errors shown in these figures are the square root of the average number of photoelectrons. The total uncertainty introduced by a small number of telescopes participating in the measurement combined with event-to-event fluctuations can be significantly greater. The fluctuations can be especially large near (< 50 m) the core. At these distances the light intensity is sensitive to the structure from multiple π° s initiating EAS cascades. Calculations further indicate that in the 10–200 TeV range, the light yield at a fixed distance from the core scales linearly with energy [23].

The simulated time of arrival of the wave front along a horizontal axis (as viewed edge on) for 36° incidence is shown in Fig. 4. This figure represents the average

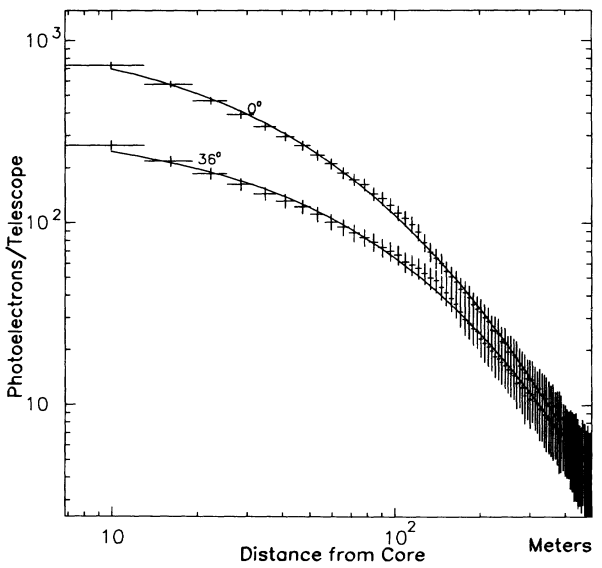

FIG. 3. Monte Carlo–generated photoelectron (per GRACE telescope) lateral distribution for vertically incident, 20 TeV protons and for 36° incidence. In both cases the telescopes are oriented along the shower axis. Lines are a parametrized fit.

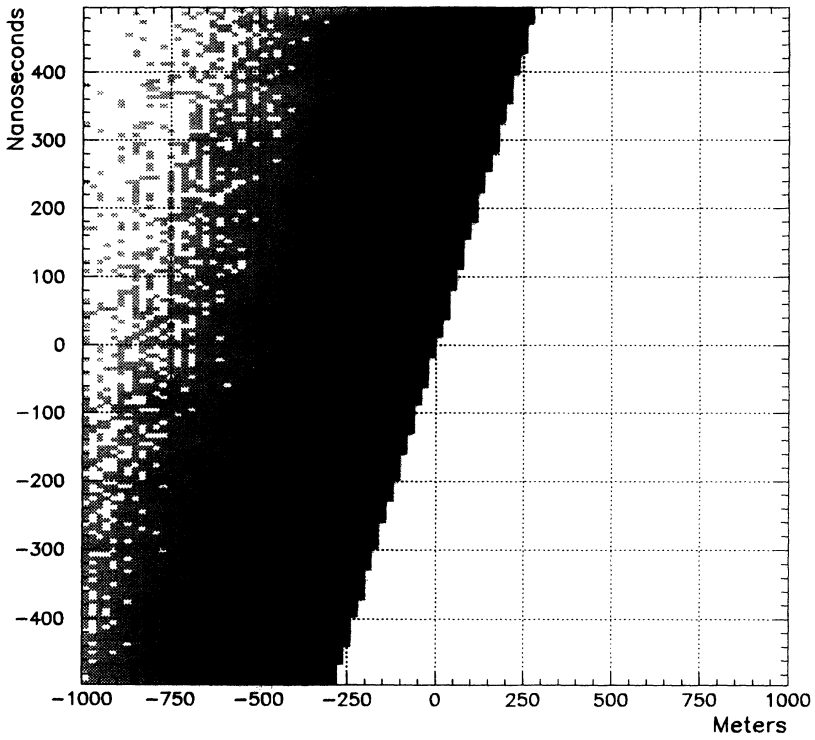

FIG. 4. Arrival time versus spatial location of wave front in side view for 36° incidence. The grey scale shows the relative density of photoelectrons observed by a telescope at a given time and location.

of twenty 20 TeV proton initiated showers. While the wave front exhibits slight curvature over a distance scale of a few km (not shown), for the much smaller distances relevant to the GRACE base lines, the wave front is essentially conical with an opening angle of about 1.3°. We show an example of a simulated signal at 100 m and 200 m from the core for a shower initiated by a 20 TeV, vertically incident proton in Figs. 5(a) and 5(b), respectively. The characteristics (i.e., rise time, width) of these pulses are similar to earlier calculations [27].

The intrinsic timing jitter is defined as the fluctuation in relative time of threshold crossing for showers incident from the same direction. The uncertainty in the measurement of the Čerenkov wave front direction depends on several factors: the trigger threshold, the length of the base line, the distance of the telescopes from the core, the shower energy, and the fluctuations in the light distribution at a fixed energy. While this jitter is difficult to calculate precisely, we conservatively estimate it by considering signals that are about 10% above threshold for two telescopes, each one 100 m from the shower core. In this case the simulated jitter per telescope is about 6 ns. The net uncertainty in arrival direction is less than 2°.

This above uncertainty can result from the fluctua-

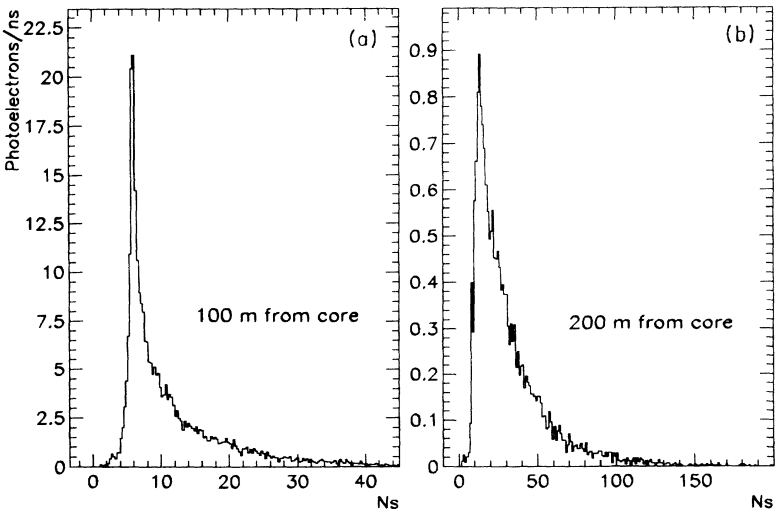

FIG. 5. Monte Carlo simulation of photoelectron arrival time distribution at (a) 100 m and (b) 200 m from the core for vertically incident proton and infinite bandwidth.

tion in path length differences taken by Čerenkov photons produced at a broad range of altitudes. For example, photons radiated by muons near the observer's altitude can arrive a few nanoseconds earlier than photons produced a few kilometers higher. A small phototube transit time jitter (measured to be less than 1 ns) also contributes to the overall timing uncertainty.

IV. RESULTS

The GRACE array acquired data on moonless and generally clear nights during the late summer and autumn of 1992. Over this period the live time (in which MACRO and GRACE were simultaneously operating) amounts to 106.1 h. Of this, 76.3 h were with six MACRO supermodules and 29.8 h were with four supermodules. We thus refer to a six supermodule effective live time of 96.2 h. In addition, two Čerenkov trigger conditions were tested: With four MACRO supermodules in operation a single telescope trigger was used, while a twofold coincidence was required with the six supermodule data. This combination of twofold and onefold triggers with six and four supermodules, respectively, was accidental.

By *clear nights* we refer to nights when stars were clearly visible, although sometimes through a discernible haze. Several nights of data acquisition were hampered by partial cloudiness, thunderstorm activity, and light pollution from vehicles and other local sources. No specifically quantifiable measure of the sky's atmospheric transmission was performed. However, the overall trigger rate at a constant gain and threshold is sensitive to fluctuations in transparency and sky brightness. In particular, during periods of partially overcast skies the trigger rate could vary precipitously when the field of view was partially obscured. In Fig. 6 are examples of trigger rates versus run time for two nights, one clear and one partially cloudy.

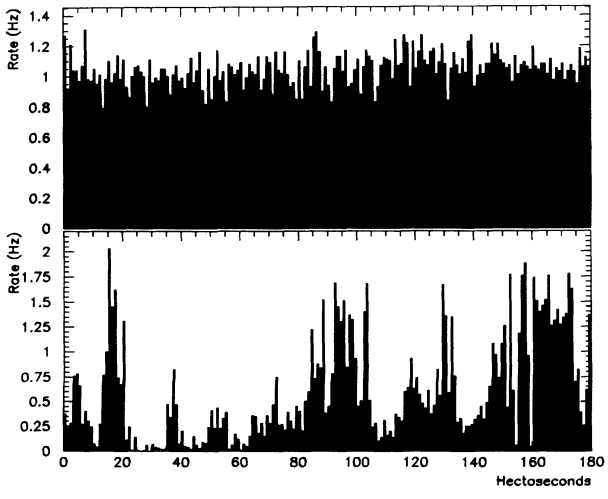

FIG. 6. Trigger rates. Top: Clear night. Bottom: partially cloudy night.

A. Noncoincident events

In order to assess the performance of the telescopes we examine the charge or photoelectron spectrum from one night's exposure. To the extent that the measured light intensity reflects the primary particle energy, the observed spectrum should reflect the primary all-particle spectrum. Distortions to this picture arise from two somewhat canceling processes. Because the light intensity falls off with radial distance from the shower core, the sensitive trigger region extending radially from a telescope increases with energy. Higher primary energy events whose core are observed farther from the telescope than nearby low energy events contribute preferentially to the low end of the charge spectrum. This tends to steepen the observed spectra. Conversely, due to the steepness of the spectrum, photoelectron fluctuations preferentially shift events from lower bins to the less occupied higher charge bins. This renders the spectrum somewhat flatter.

The conversion of charge spectrum to cosmic ray energy spectrum has previously been done from the Monte Carlo–simulated charge distributions for each shower energy [28]. A result of this work is that that the observed charge spectrum has the same power law index as the primary spectrum.

The Monte Carlo simulation used in this work is tailored to the specific trigger conditions of the run. This simulation samples a primary energy from the all-particle spectrum measured by the Akeno detector [29] (differential spectral index=2.62±0.12) and uniformly distributes

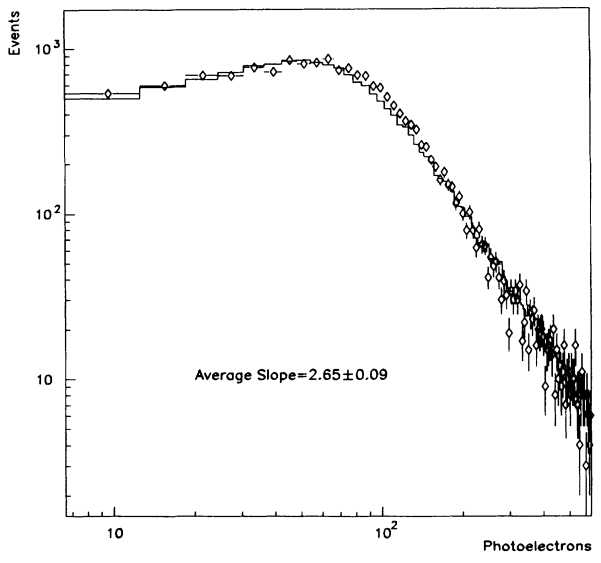

FIG. 7. A typical spectrum from a single run for non-coincident events. Solid line: Monte Carlo result normalized to the number of events in the data. Underflow and overflow events are omitted. The slope is the parameter in a power law fit to the tail of the spectrum. The slope reported is the average of the five telescope spectra.

cores in a region extending to 500 m from the center of the array. The light intensity is determined according to the 36° incidence radial distribution in Fig. 3, where we have assumed, based on earlier work [23], that the intensity at a given radial distance scales linearly with primary energy. For shower cores off the optical axis, an appropriate correction is made to account for a telescope's reduced geometrical acceptance. The actual number of photoelectrons is then sampled from a Gaussian or Poisson distribution whose width is determined by photoelectron statistics and the event-to-event fluctuation in light intensity. Included are pedestal level fluctuations that presumably result from the quasiconstant ambient light of the night sky. The average measured amplitude of the fluctuations is 24 ± 11 photoelectrons. This statistical error reflects the spread of the average fluctuation and the random uncertainty in the calibration of the ADC. We estimate an additional systematic error in the ADC bins to photoelectron conversion to be $\sim 30\%$. A representative spectrum from one night's run is shown in Fig. 7 with our Monte Carlo simulation. The slope and error quoted in the figure represents the average spectrum of five telescopes. The power law fit is made to the tail of the distribution and is consistent both with the simulation and with the cosmic ray all-particle spectrum.

B. Coincident Events

A surface-underground event time difference histogram (Fig. 8) from one run employing a twofold trigger shows the event correlation peak for increasingly confining spatial cuts on the core location. The timing resolution (one standard deviation) displayed by these peaks is 50 μs, obtained after correction for a smooth, thermal clock drift. The offset of the peak from zero reflects only the relative absolute times on the GRACE and MACRO clocks and has no special significance. For some runs, particularly those in which the temperature swings in our unheated counting house were extreme (subfreezing to $\sim 20\,^{\circ}$C), thermal clock corrections were not possible. These three runs employed single telescope triggering, admitted the highest rates, and enjoyed the longest nights. The timing widths for these runs were between 1 and 2 ms. The data cuts shown in Fig. 8 require that the shower cores fall within a specified region around the array. Core locations are determined by extrapolation of MACRO muon tracks to the surface of the array. Events that fall within two standard deviations from the peak (with the 200 m cut imposed) are considered coincidences. In Fig. 8 this coincident window is 100 μs. The background contribution to the peak is taken to be the average bin occupancy of the histogram. It is apparent that for core location cuts less than 200 m, the number of events in the peak diminishes according to reduction in background. The 200 m limit, beyond which few if any coincident events are seen, is consistent with the maximum angular opening of the telescope aperture, and the requirement that a muon track point towards MACRO.

The MACRO-determined spatial locations of all coincidence events (as defined above) on a plane level with the center of the array are shown in Fig. 9. The locations of the telescopes are indicated by stars, and the centroid of these events is marked by the small box near

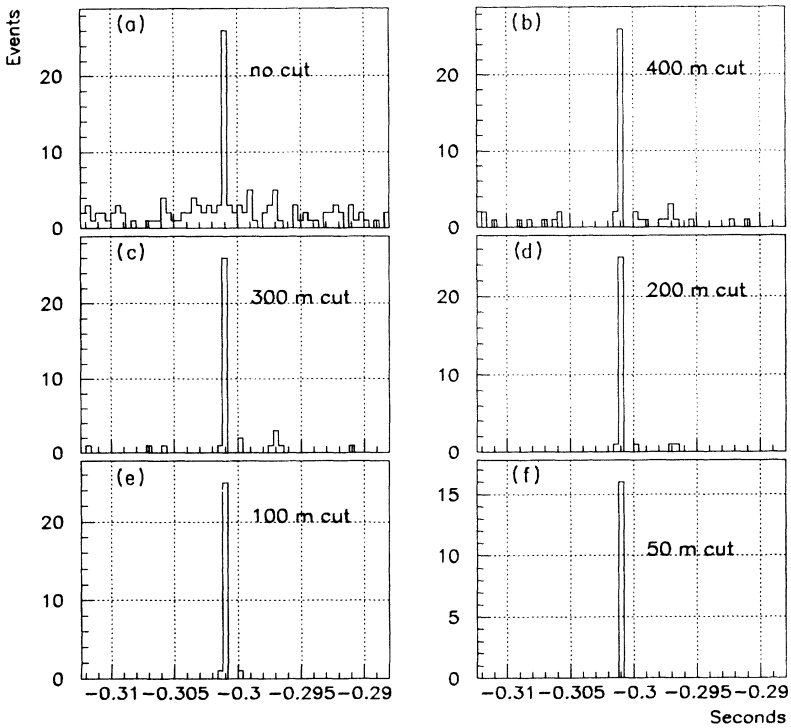

FIG. 8. Typical surface-underground timing peak for various spatial cuts on the location of shower core as determined by MACRO. For clarity the 400 μs bin size is chosen that all coincident events fall in a single bin. The offset from zero is due to the absolute time difference between surface and underground detectors. (a) No cut. (b) Core within 400 m of perimeter of GRACE. (c) 300 m (d) 200 m (e) 100 m (f) 50 m.

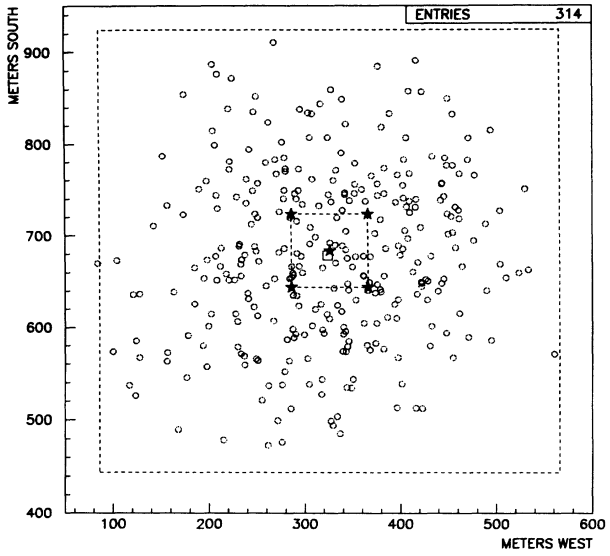

FIG. 9. Location of coincident events determined from MACRO muon tracks extrapolated to surface. The random uncertainty in the positions is $\sim$ 20 m. The box indicates the location of the centroid of all events and its width shows one standard deviation of the mean.

the array's center. The size of the box corresponds to the random uncertainty. The outer dotted line shows the 200 m data selection boundary: Tracks external to this boundary are unlikely to be coincidence events. It is clearly evident that most events cluster near the array.

The background contribution for several runs is quite small. In Fig. 8(d), for example, there are 647 events distributed over 5000 bins (the full range of which is not shown) to give an average background occupancy of 0.13 events per bin. As there are over 20 events in the peak bin, the background contribution in this particular run is under 1%. However, some runs had relatively high irreducible backgrounds. Notably, as mentioned earlier, the three runs in which a single telescope trigger was employed had wide (1–2 ms) timing peaks, coupled with the higher trigger rates. As a consequence the signal to background ratio was not as good as earlier runs. Because of the longer live time of these runs ($\sim$ 10 h each), however, they provided a significant fraction of the total coincident event sample, some 93 events. Of these, 13.7% are likely accidental coincidences. For our overall data sample of 321 coincident events the average background contribution is 9.5%.

C. Efficiency and energy threshold

We define the efficiency as

$$\epsilon(r, n_\mu) = N_{\rm coinc}(r, n_\mu)/N_{\rm MACRO}(r, n_\mu), \qquad (1)$$

where $N_{\rm MACRO}(r, n_\mu)$ is the the number of events of muon multiplicity $\geq n_\mu$ that point back to within a radius r from the center of the surface array, and $N_{\rm coinc}$ is the number of these events generating surface triggers. This efficiency must clearly depend on the radius, since at some sufficiently large distance no coincidence events would be detected. With this definition, the efficiency curve for all detected multiplicities is shown in Fig. 10. Data are shown separately for runs using the two and single telescope trigger condition. Excluded data are runs on nights when the sky was partially occluded, and from the first three runs whose trigger thresholds were set significantly higher than on following nights. The electronic thresholds for the singlefold trigger runs was set 2–3 times higher than in the other runs. This results in a reduced efficiency for regions close to the array compared with the two telescope trigger. Otherwise, the single telescope trigger efficiency is almost constant out to 200 m.

We can estimate the air Čerenkov array's energy threshold by comparing its measured efficiency with the calculated fraction of underground muon events above a certain energy. At the energies of interest, $<$ 100 TeV, the dominant progenitors of penetrating muons are cosmic ray protons with an energy higher than the minimum required for a muon to reach detector depth. This energy is given by [9] E_μ [TeV] $= (0.53e^{0.4h} - 1)$ where h is the slant depth from the surface to the detector in units of 1000 mwe. The slant depth of MACRO (from GRACE) is $\sim$ 3400 mwe, and so $E_\mu = 1.5$ TeV. To obtain the fraction of events above a given energy at 3400 mwe and for the GRACE-MACRO zenith angle of 36°, we use a Monte Carlo calculation of the deep underground muon flux detected in MACRO described in Ref. [2]. In this calculation, the probability for at least one muon to reach detector depth is determined from negative binomial statistics and folded with the cosmic ray spectra for different elemental species, the detector's geometrical acceptance, trigger, and track reconstruction efficiencies. Figure 11 shows the integral energy distribution for muon events in MACRO generated by a light primary compo-

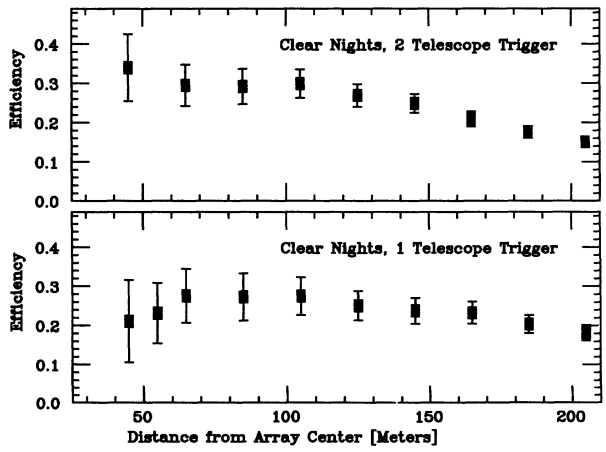

FIG. 10. GRACE trigger efficiency versus core distance from the center of the array. Top: Data include runs employing a two telescope trigger, exclusive of those on partially cloudy nights. Bottom: single telescope trigger condition.

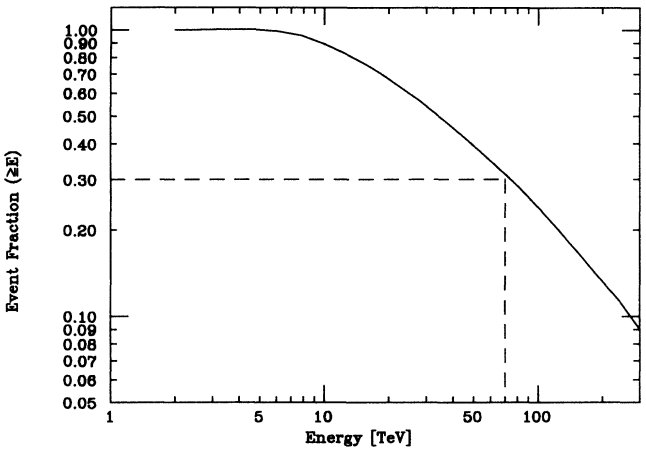

FIG. 11. Monte Carlo–determined fraction of muon events in MACRO initiated by a primary nucleus with energy greater than 2 TeV as a function of energy. The dashed line indicates the fraction of events that trigger GRACE on the ordinate axis and on the abscissa the corresponding energy threshold, assuming a step function turn on.

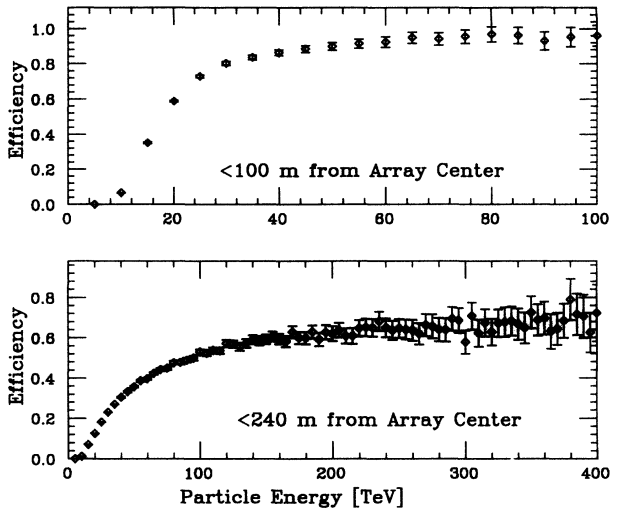

FIG. 12. Monte Carlo–simulated GRACE trigger efficiency. Top: for cores < 100 m from array center. Bottom: < 240 m.

sition model [30] in which protons are the dominant component. Also shown in this figure is the Čerenkov array's efficiency for events falling within 100 m of the array's center. We choose the efficiency at this point because in a conceivable expanded array, most events would likely fall within this distance of a telescope. According to Fig. 11 essentially 100% of MACRO muons arise from primary energies above $\sim$ 2 TeV, and 24% of them derive from an energy above 100 TeV. By association of the GRACE efficiency with a fraction of the underground muon flux, we might conclude that the array triggers with essentially 100% efficiency at $\sim$70 TeV. However, the trigger threshold is probably not monoenergetic, but increases from zero at some nominal energy and rises to saturation. This smearing of the threshold would result from the fluctuations in the Čerenkov light intensity for showers initiated by monoenergetic primaries. In the absence of a precise knowledge of the threshold function (which we estimate in the following paragraph) and given an efficiency of $0.3 \pm .04$ we can interpret Figs. 10 and 11 to indicate that GRACE triggers with 100% efficiency in the region 60–100 TeV, but the actual "turn on" (e.g., 10% trigger efficiency) occurs well below this energy.

We can derive an independent estimate of the GRACE primary energy threshold from the Monte Carlo described in the earlier noncoincident events section. The trigger level (which we initially estimated to be in the 30–50 photoelectron range, depending upon the particular telescope) is a free parameter in the simulation. We exploit this to obtain improved estimates of the telescopes' trigger thresholds by requiring that the peaks and onset of the power law spectrum of the measured and simulated distributions be in agreement. From this procedure, we obtain a telescope averaged threshold of 52 ± 9 photoelectrons. An additional $\sim$30% systematic uncertainty in the gain calibration contributes to the uncertainty. With the thresholds determined, the estimated trigger efficiency versus primary energy (for shower cores restricted to within 100 m and 240 m of the array center) is shown in Fig. 12. For the 100 m curve, the trigger efficiency saturates at $\sim$ 90 TeV. Furthermore, according to this estimate, the Čerenkov array triggers with 50% efficiency at $\sim$20 TeV.

The result in Fig. 12 predicts a high efficiency ($\sim$90%) at 50 TeV. This is somewhat less than the threshold derived from the relative trigger rates of the surface and underground detector. However, the threshold obtained by the method could be underestimated. Possible systematic uncertainties inherent in the Monte Carlo calculation may exaggerate the photoelectron yield. In particular, the simulation assumes an ideal atmospheric profile, not necessarily adapted to the specific environment (sometimes hazy) in which our telescopes resided. Additional unmeasured (and hence unquantifiable effects) such as dust and/or dew condensation on the telescope covers may have further diminished the light collection.

To summarize, the primary energy threshold, which we may define as the point at which GRACE triggers with 50% efficiency, probably lies between the results of the two methods. The former method is consistent with 100% efficiency at 60–100 TeV but assumes a step-function-like turn on and gives no information on the threshold function. The latter method indicates a 50% trigger efficiency $\sim$ 20 TeV with full efficiency above 90 TeV.

D. Lateral distribution of light

The lateral distribution of Čerenkov photons is the convolution of several stochastic air shower processes: the interaction (and inelasticity thereof) of the primary

nucleus, the production multiplicity and transverse momentum distribution of pions, the evolution of the electron cascade, and the atmospheric attenuation of light. Previous efforts [31–34] have obtained some agreement between early calculations of the lateral distribution and experiment. These measurements, performed in conjunction with EAS arrays, examine the pulse height normalized to the electron density versus the core distance where the latter is determined from the EAS data.

To some extent we are able to directly assess the Monte Carlo–generated lateral distribution of photoelectrons. To do this, we use the location of the core which is approximated from the underground muon track together with the total charge observed by each telescope. Although the number of coincidences is not large, we can exploit the fact that for each event there is often more than one pair of telescopes participating. In this analysis we use the 1159 telescope pair combinations from the entire coincidence event sample.

In Fig. 13 the logarithm of the phototube pulse charge ratio for each such pair is plotted against the logarithm of the ratio of the telescope to core distances. Data at the extremes of this curve are excluded because of very large uncertainties. These correspond to shower cores projected to fall < 10 m from a telescope. This curve is sensitive to the radial distribution of Čerenkov light. The use of charge (or photoelectron) ratios removes the dependence on the shower energy as well as artifacts caused by nightly variations in gains. In this plot the gains have been normalized separately for each run. We note that if the gains are not normalized, the basic shape of the curve would not change; it would be smeared (up or down) along the coordinate axis by an amount equal to the variations of the logarithm of the gain ratio.

Also shown in Fig. 13 are two simulation results obtained from the Monte Carlo calculation described in the spectrum of noncoincident events section. In the calculation the core distance is constrained to be less than 200 m from the perimeter of the array in order to correspond to the real data selection. We have considered both the "vertical" incidence and 36° lateral distributions via the parametrizations of the curves in Fig. 3. These parametrizations are $n_{\rm pe} = 1155.0 r^{-0.3019+0.1076\times\ln(r)-0.0333\ln^2(r)}$ for the 36° incidence angle and $n_{\rm pe} = 593.7 \times r^{-0.7558+0.2573\ln(r)-0.043\ln^2(r)}$ for vertically incident showers. Here $n_{\rm pe}$ is the photoelectron yield and r is the distance of the telescope to the core. For these two shower directions the telescopes are taken to point along the shower axis. Therefore a change in angle corresponds to a change in the effective atmospheric slant depth.

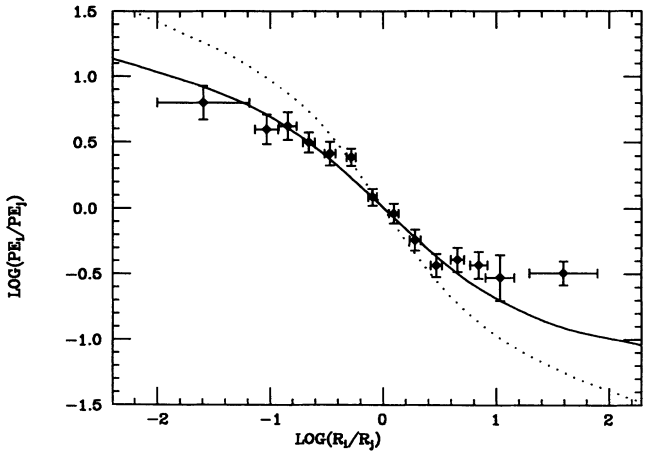

FIG. 13. Logarithm of photoelectron ratio versus the logarithm of core distance ratio for all telescope pair combinations (indicated by indices i and j) for all coincident events. Solid line: Monte Carlo result using 36° photoelectron lateral distribution. Dotted line: Monte Carlo simulation for 0° incidence photoelectron lateral distribution.

It is evident that there exists at least qualitative agreement between the observed data and the Monte Carlo simulations for the case where showers arrive from 36°. The χ^2 of the data and Monte Carlo for the 36° shower is $1.8/N_{\rm DF}$ (for 14 degrees of freedom), while the vertically incident lateral distribution produces a $\chi^2/N_{\rm DF}$=5.4. The flattening at either end of the observed curve is possibly due to phototube saturation. We conclude that the 36° lateral distribution of Čerenkov photoelectrons is marginally consistent with our observations. Other than the phototube gain normalization which was determined by the data, there are no free parameters in the Monte Carlo input. Our fundamental approximation is that the general shape of the lateral distribution is, within the 10^{13}–10^{14} eV energy range where our coincidence events are most likely to occur, independent of the primary particle energy.

E. Multiple muon events

While the high statistics required for multiple muon composition studies are not attained in our data sample, it is nevertheless interesting to examine the coincident event multiplicity distribution in comparison to Monte Carlo calculations for a light composition model [30] used in a previous paper [2]. For a comparison consistent with the parameters of the Monte Carlo calculation, all six MACRO supermodules were required to be operational. This excludes the final three MACRO/GRACE runs in which only four supermodules were on line. We use here all multiple muon events whose cores extend to 240 m from the array perimeter. With these restrictions, the total MACRO data set consists of 2062 events; the GRACE coincidence data include 166 events. In this case GRACE triggers on approximately 8% of the MACRO events whose tracks pass through this area. According to the Monte Carlo result in Fig. 12, the Čerenkov array threshold for events out to this distance increases very slowly and is 60% efficient above $\sim$ 200 TeV. While there is some uncertainty in the threshold, it must be significantly higher for this extended region simply because most events fall far from the telescopes. Consequently a richer contribution of multiple muon bundles (which reflect higher energy primaries) is expected in the coincident event data ($\sim$ 20% of the single muon content)

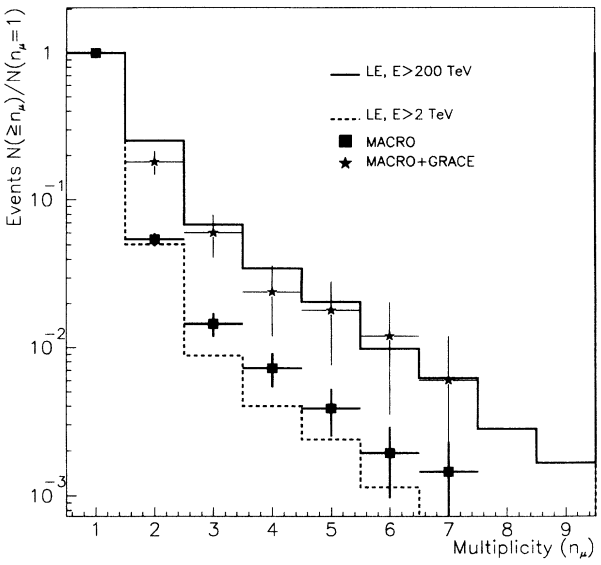

FIG. 14. Integral muon multiplicities observed by MACRO during GRACE operation. Data represent muon bundles whose core passes within 200 m of the perimeter of the surface array. Stars represent coincidence events. Histograms are Monte Carlo data.

than in the MACRO only data ($\sim 6\%$ of the single muon content). Figure 14 shows the observed integral multiple muon frequency distribution for all MACRO events passing within the GRACE region, and for the coincident sample. The data have been normalized, to the total number of events, 2062 and 166, respectively, in each distribution. We also show HEMAS-based [13] Monte Carlo simulation results using a light model for the cosmic ray composition [30]. This model has been previously shown to be preferred over a heavier composition with two [2] and six [35] supermodule MACRO data. Based on an approximated GRACE threshold of 200 TeV, Fig. 14 shows the light composition result produced by nuclei above this energy. While this model is modestly compatible with our data, no conclusion is possible due to the paucity of events coupled with Monte Carlo uncertainties.

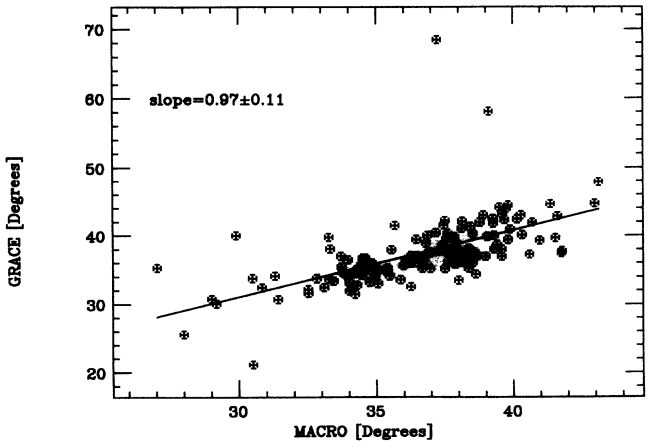

FIG. 15. GRACE versus MACRO zenith angle.

F. Measurement of shower direction

The relative time of arrival of the Čerenkov light cone at each station can yield the arrival direction of the shower. While Monte Carlo simulations discussed earlier indicate that the angular resolution for single events is limited to about 1.5°, mainly due to fluctuations in the arriving wave front, a sample of coincident events can be used to obtain a measure of the pointing precision of an underground detector. The arrival direction is calculated by minimization of

$$\chi^2 = \sum_j [ct_j + \epsilon_j(r_j) + n(\theta,\phi)\cdot \mathbf{s}_j]^2 \qquad (2)$$

where $\mathbf{n}(\theta,\phi)$ is the direction unit vector of the wave front, t_j and $\mathbf{s}_j$ are the pulse arrival times and location of the station j relative to the origin respectively. ϵ_j is a small correction for the conical shape of the wave front that depends on the distance from the core, $\mathbf{r}_j$. A slewing or time-walk correction is included, which removes the dependence on pulse amplitude of the threshold crossing time.

The relative timing offsets between pairs of telescopes are obtained from the calculated average arrival time difference of all wave fronts that trigger the pair. This calibration is based on the measured pointing direction of the optical axes. The systematic uncertainty in this procedure is obtained from the estimated systematic errors in the zenith and azimuthal angle orientations of the telescopes, 0.2° and 0.25°, respectively.

In Fig. 15 we show the GRACE versus MACRO zenith angles. The slope of the linear fit is 0.97±0.11 Figs. 16(a)

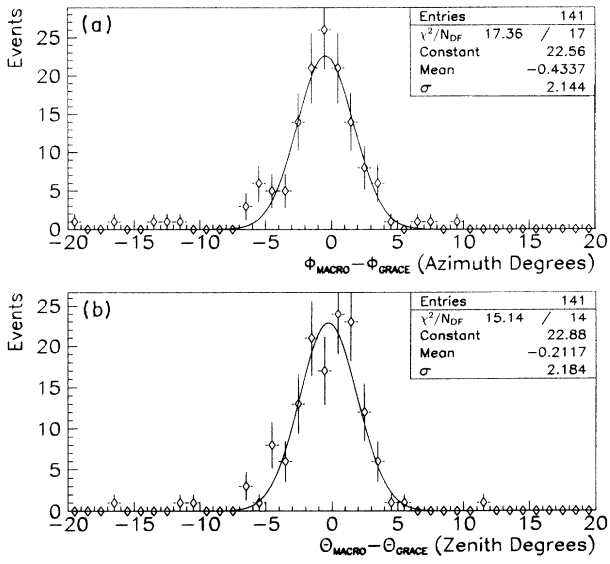

FIG. 16. Difference of MACRO from GRACE: (a) azimuthal angle, (b) zenith angle.

and 16(b) show the difference in azimuthal and zenith angles as measured by the two detectors. The known systematic uncertainty in the array's determination of arrival direction is $\sim 0.5°$. This is determined from the estimated systematic uncertainty in the timing offsets which is in turn established by the uncertainty in the orientation of the optical axes of the telescopes. The observed difference of MACRO and GRACE pointing can be accounted for by this systematic uncertainty and the 0.2° random error.

V. CONCLUSION

The goal of this work has been to establish the desirability of operation of an air Čerenkov array coupled with a deep underground muon detector. Through such an experiment we hope to provide motivation and evidence that an expanded large scale array can be a useful tool for the continued study of high energy cosmic ray interactions and composition. With the modest and inexpensive array employed for this measurement we have obtained results consistent with the Monte Carlo–predicted radial distribution of Čerenkov photons in an EAS. We estimate that this array has triggered with $\sim 50\%$ efficiency in the range of 20–50 TeV. This coincidence technique is therefore potentially useful as a tool to study high energy, high rapidity events initiated by protons on air.

Additionally, our ~ 300 event sample includes 166 events with six MACRO supermodules in operation, and contains more than 40 multiple muon events collected within a radial distance of 240 m from the array center. We have estimated the trigger efficiency for these events to be $\sim 60\%$ at 200 TeV. Although the number of such events is too small to extract significant results on the cosmic ray composition, particularly at higher energy, we note that these initial observations of deep underground multiple muons with air Čerenkov radiation in extensive air showers encourage continued efforts to study high energy cosmic ray interactions and composition by means of simultaneous observations of different EAS components.

ACKNOWLEDGMENTS

We are deeply indebted to the former Gran Sasso Laboratory director Professor E. Bellotti and staff for their extensive cooperation and assistance for this work. We are grateful to J. Gaidos at Purdue University for ideas on telescope construction, and for providing mirrors for this experiment. We further acknowledge funding provided by the U.S. Department of Energy, the National Science Foundation, and the University of Michigan Phoenix Memorial Reactor.

[1] V.L. Ginzburg and S.I. Syrovatskii, *The Origin of the Cosmic Rays*, English ed. (Pergamon Press, New York, 1964), p. 49.
[2] MACRO Collaboration, S.P. Ahlen *et al.*, Phys. Rev. D **46,** 4836 (1992).
[3] D. Cebula *et al.*, Astrophys. J. **358,** 637 (1990).
[4] Soudan 2 Collaboration, J.L. Thorn *et al.*, Nucl. Instrum. Methods **283,** 642 (1989).
[5] LVD Collaboration, C. Bari *et al.*, Nucl. Instrum. Methods A **264,** 5 (1988).
[6] Frejus Collaboration, C.H. Berger *et al.*, Phys. Rev. D **40,** 2163 (1989).
[7] NUSEX Collaboration, G. Bologna *et al.*, Nuovo Cimento C **8,** 76 (1985); also M. Aglietta *et al.*, in *Astrophysics and Particle Physics,* Proceedings of the Topical Seminar, San Miniato, Italy, 1989, edited by G. Castellini *et al.* [Nucl. Phys. B (Proc. Suppl.) **14B**, 193 (1990)].
[8] Baksan Collaboration, E.N. Alexyev *et al.*, in *Proceedings of the Sixteenth International Conference on Cosmic Rays*, Kyoto, Japan, 1979, edited by S. Miyake (University of Tokyo, Tokyo, 1979), Vol. 10, p. 276.
[9] T.K. Gaisser and Todor Stanev, Nucl. Instrum. Methods **A235,** 183 (1985).
[10] T. Gaisser, *Cosmic Rays and Particle Physics* (Cambridge University Press, Cambridge, England, 1990), p. 51.
[11] J. Wdowczyk and A. W. Wolfendale, Nature (London) **306,** 347 (1983); also Nuovo Cimento A **54,** 433 (1983).
[12] J.W. Elbert, T.K. Gaisser, and T. Stanev, Phys. Rev. D **27,** 7 (1983).
[13] C. Forti *et al.*, Phys. Rev. D **42,** 3668 (1990).
[14] M. Simon *et al.*, Astrophys. J. **239**, 712 (1980).
[15] EASTOP and LVD Collaborations, M. Aglietta *et al.*, Nuovo Cimento A **105**, 1807 (1992); **105**, 1815 (1992).
[16] EASTOP and MACRO Collaborations, in *Proceedings of the Second International Workshop on Neutrino Telescopes,* Venice, Italy, 1990, edited by M. Baldo-Ceolin (University of Padua, Padua, 1990), p. 209.
[17] W. Galbraith, *Extensive Air Showers* (Butterworth Scientific Publications, London, 1985), p. 189.
[18] The MACRO and EASTOP Collaborations, R. Bellotti *et al.*, Phys. Rev. D. **46**, 4836 (1990).
[19] U. DasGupta, T.H. Fields, and K. Ruddick, in *Proceedings of the 22nd International Cosmic Ray Conference*, Dublin, Ireland, 1991, edited by M. Cawley *et al.* (Dublin Institute for Advanced Studies, Dublin, 1992), paper OG 6.1.14.
[20] P. Sokolsky, *Introduction to Ultrahigh Energy Cosmic Ray Physics* (Addison-Wesley, Menlo Park, CA, 1989), p. 39.
[21] M. Calichio *et al.*, Nucl. Instrum. Methods A **264,** 18 (1988).
[22] MACRO Collaboration, S.P. Ahlen *et al.*, Nucl. Instrum. Methods A **324,** 337 (1993).
[23] D.S. Levin *et al.*, Nucl. Instrum. Methods A **322,** 101 (1992).
[24] GRACE mirrors are of the type used in the Haleakala Gamma Ray Observatory.
[25] The MACRO Collaboration, S.P. Ahlen *et al.*, Astrophys. J. **412**, 301 (1993).
[26] M. Kertzman and G. Sembroski, Nucl. Instrum. Methods A **343**, 629 (1994).

[27] T.J. McComb and K.E. Turver, Nuovo Cimento C **5**, 2 (1982).
[28] D.H. Hartman *et al.*, Nuovo Cimento A **51,** 1 (1979).
[29] M. Nagano *et al.*, in *Proceedings of the 22nd International Cosmic Ray Conference* [19], paper HE 1.4.
[30] G. Auriemma, T. Gaisser, and T. Stanev, in *Proceedings of the 21nd International Cosmic Ray Conference,* Adelaide, Australia, 1989, edited by R.J. Protheroe (Graphic Services, Northfield, South Australia, 1990), paper HE 4.5-5.
[31] I.P. Ivanenko *et al.*, in *Proceedings of the Sixteenth International Conference on Cosmic Rays* [8], Vol. 9, paper EA4-12.
[32] G.J. Smith and K.E. Turver, J. Phys. A **6**, L121 (1973).
[33] C. Castagnoli *et al.*, Nucl. Phys. **B2**, 369 (1967).
[34] V.I. Zatsepin and A.E. Chudakov, Sov. Phys. JETP **15,** 1126 (1962).
[35] The MACRO Collaboration, in *Proceedings of the 23rd International Cosmic Ray Conference*, Calgary, Canada, 1993, edited by D. A. Leahy (University of Calgary, Calgary, 1993), paper OG 6.4.3.

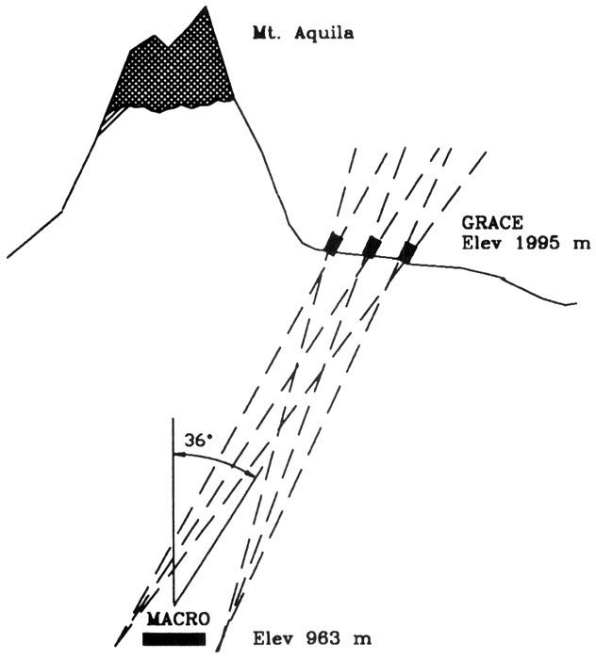

FIG. 2. Profile of GRACE-MACRO configuration.

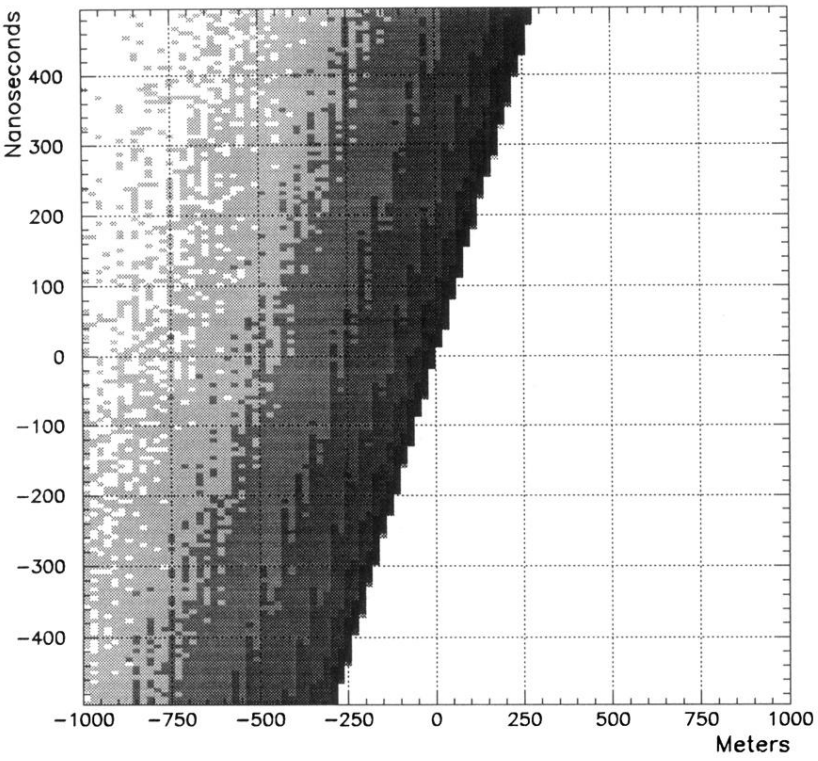

FIG. 4. Arrival time versus spatial location of wave front in side view for 36° incidence. The grey scale shows the relative density of photoelectrons observed by a telescope at a given time and location.

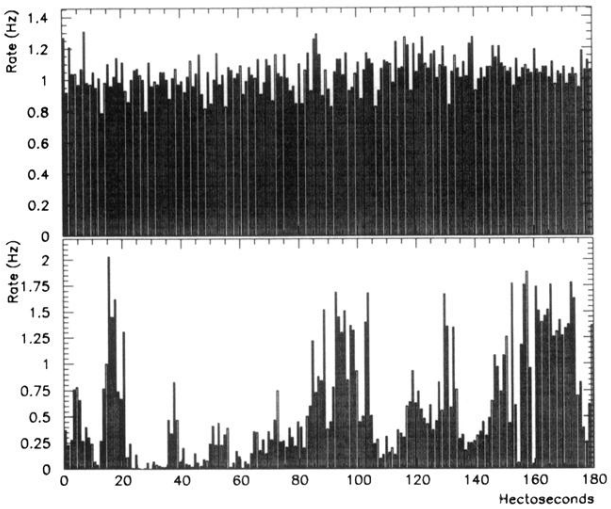

FIG. 6. Trigger rates. Top: Clear night. Bottom: partially cloudy night.